



Core Models of Receptor Reactions to Evaluate Basic Pathway Designs Enabling Heterogeneous Commitments to Apoptosis

Marielle Péré, Madalena Chaves, Jérémie Roux

► To cite this version:

Marielle Péré, Madalena Chaves, Jérémie Roux. Core Models of Receptor Reactions to Evaluate Basic Pathway Designs Enabling Heterogeneous Commitments to Apoptosis. CMSB 2020 - 18th International Conference on Computational Methods in Systems Biology, Sep 2020, Konstanz, Germany. pp.298-320, 10.1007/978-3-030-60327-4_16 . hal-03021538

HAL Id: hal-03021538

<https://hal.science/hal-03021538>

Submitted on 2 Dec 2020

HAL is a multi-disciplinary open access archive for the deposit and dissemination of scientific research documents, whether they are published or not. The documents may come from teaching and research institutions in France or abroad, or from public or private research centers.

L'archive ouverte pluridisciplinaire **HAL**, est destinée au dépôt et à la diffusion de documents scientifiques de niveau recherche, publiés ou non, émanant des établissements d'enseignement et de recherche français ou étrangers, des laboratoires publics ou privés.

Core models of receptor reactions to evaluate basic pathway designs enabling heterogeneous commitments to apoptosis

Marielle Péré^{1,2}, Madalena Chaves¹, and Jérémie Roux^{1,2}

¹ Université Côte d’Azur, Inria, INRAE, CNRS, Sorbonne Université, Biocore team, Sophia Antipolis, France

² Université Côte d’Azur, CNRS UMR 7284, Inserm U 1081, Institut de Recherche sur le Cancer et le Vieillissement de Nice, Centre Antoine Lacassagne, 06107 Nice, France

Abstract. Isogenic cells can respond differently to cytotoxic drugs, such as the tumor necrosis factor-related apoptosis inducing ligand (TRAIL), with only a fraction committing to apoptosis. Since non-genetic transient resistance to TRAIL has been shown to dependent on caspase-8 dynamics at the receptor level *in vitro*, here we investigate the core reactions leading to caspase-8 activation, based on mass-action kinetics models, to evaluate the basic mechanisms giving rise to the observed heterogeneous response. In this work, we fit our models to single-cell trajectories of time-resolved caspase-8 activation measured in clonal cells after treatment with TRAIL. Then, we analyse our results to assess the relevance of each model and evaluate how well it captures the extent of biological heterogeneity observed *in vitro*. Particularly, we focus on a positive feedback loop on caspase-8, the impacts of initial condition variations and the relevance of the caspase-8 degradation.

Keywords: ODE · Mass-action kinetics · Parameter identification · Apoptosis · Fractional killing · TRAIL · Caspase-8.

1 Introduction

Apoptosis plays a key role in human tissue homeostasis. Its disruption causes well-known diseases such as Alzheimer, Parkinson (excessive apoptosis), or autoimmune disorders and cancers (lack of apoptosis).

To induce cell death in tumor cells, many treatments have been designed and tested so far, such as TRAIL-receptor ligands, which present the advantage of sparing healthy cells. TRAIL binds the death receptors (DR4/5) of the cancer cell, initiating the extrinsic apoptosis pathway. Then, a Death-Inducing Signaling Complex (DISC) is formed in the cytoplasm with adaptor-proteins such as FADD (Fas-Associated protein with Death Domain). This association allows the recruitment of the pro-caspase 8 and 10 (hereafter pC8 and pC10) and other proteins. These pro-caspases compete at the DISC level with c-FLIP [8], an anti-apoptotic protein, to activate the initiator caspase 8 (C8) [31] via

dimerization (or even trimerization) and self-cleavage of pC8 [19]. In many cell types, once activated, C8 triggers cell death by mediating Bid cleavage causing the mitochondrial outer membrane permeabilization (MOMP, [4]) which induces the activation of the effective caspases 3 and 7 (C3 and C7), or “executioner caspase”, leading to DNA fragmentation and cell death [21,30].

Although TRAIL has been a very promising drug thanks to its ability to target cancer cells specifically, it showed only limited success in the clinic due to a lack of efficiency. In fact, single-cell studies revealed that cells from the same clonal population commit differently to cell death when treated with TRAIL (or other pro-apoptotic drugs), with an important variability in the time of death for the sensitive cells and with a fraction of cells evading apoptosis entirely. When the remaining resistant cells are retreated a second time with cancer drugs (even saturating doses), fractional killing is once again observed. [32,33].

A number of studies and mathematical modeling efforts have evaluated the origins of drug response heterogeneity, proposing mechanisms such as the random fixation of TRAIL on the DR4/5 [1,3], the presence of decoy receptors (which impair the formation of a functional DISC after ligand binding [2]) or the p53 gene effects on TRAIL efficiency [24,25]. The gene CD-95 has also an impact as it regulates FADD, an essential protein for the pC8 binding to the DISC [5,26,27,28]. c-FLIP antagonist role has been revealed as well, and gives a better understanding of how it “competes” with pC8 at DISC level to trigger (or not) apoptosis [9,6,7,5], (even if C8 and FLIP seem to bind the DISC on different sites, pC8 favors c-FLIP recruitment [8]). The action of C10 is less well identified. It may be an anti-apoptotic factor in some cases [10], as some members of Bcl-2 family that competes for activating MOMP downstream [30,21,4]. But C10 has also a pro-death role [11,12], it can trigger apoptosis in absence of C8 [13,14] and favor anti-tumorigenesis [15]. Finally, C8 activation has been defined as a determining factor in cell death decision [16], by showing a threshold in rate and timing for C8 activation that distinguishes resistant and sensitive cells [17].

These studies lead to the conclusion that cell decision happens before MOMP and the effector caspase cascade.

Here, taking these insights into consideration with C8 threshold as the main determinant of cell fate, we aim to identify within the core reactions, basic pathway designs that capture cell response heterogeneity to TRAIL, and features of C8 dynamics. Once identified, the next goal is to characterize these regulatory events, to understand how and to what extent, some proteins may influence the C8 dynamic and determine how their variation is correlated to the cell-to-cell variability.

In that aim, we especially focus on three points: (i) FADD role and its capacity for regulating C8, (ii) the relevance of caspase clusters composed of C8 and C10, and (iii) the regulatory effect of the effector caspases on C8 which depends on a positive feedback loop. To investigate the effect of these interactions and their relative timing on apoptosis, we then propose four alternative minimal ODE models. Next, based on the results of Roux and al. [17], these models are calibrated from single-cell data and the distributions of the different

parameters are analysed to find links between the models, the C8 dynamic and the cell fates. Finally, we study the feedback loop action, quantify the influence of FADD and C10 and validate our models, explaining the special distribution of C8 degradation.

2 Modeling the main processes of extrinsic apoptosis initiation

The first goal is to establish the mechanisms responsible for the main pathway dynamics, and their impact on the C8 activation threshold distinguishing between TRAIL resistant and sensitive cells. The second aim is to understand how these mechanistic models can reproduce cell response heterogeneity.

To this end, this study focuses on three different regulation points : the FADD protein and its capacity for regulation of C8, the importance of C8/C10 cluster in C8 activation [10] and the possible presence of a downstream regulatory effect of C8 [21,30], symbolized here by a positive feedback loop from the effector caspase cascade on the C8. In each case, our analyses aim to understand the effect of a given mechanism on the C8 dynamics main features and in which measure this process is a source of heterogeneity or, at least, source of extrinsic noise.

2.1 Models' assumptions

To capture the extrinsic apoptosis core reactions, our models are thus constructed with a minimal number of components and steps : the TRAIL binding on the death-receptor DR4/5, the recruitment of the FADD protein and the initiator pC8 to form the DISC, the pC8 dimerization, and finally the activation of C8. (c-FLIP is considered to be in very small quantities and so has a lower impact on C8 recruitment.)

TRAIL is denoted by T, the DR4/5 receptors become a single component named R (for Receptor), the pC8 and C8 are grouped to form a unique protein C8. Instead of the recruitment of a single pC8, our models assume two molecules simultaneously bind to DISC, since only dimerization or trimerization of pC8 can trigger apoptosis. F_D denotes the FADD protein and Z_0 the complex TRAIL-receptors. The downstream caspase cascade, the MOMP and cell death are grouped into the component D, with a intermediary complex Z_1 .

2.2 Extrinsic apoptosis initiation core models (EAICM)

Four extrinsic apoptosis initiation core models (EAICM) are proposed, corresponding to the four possible combinations of presence or not of a feedback loop on C8 conjugated with either the adaptor protein or C8/C10 binding.

The feedback loop is represented by the red links on Figure 1. Two models focus on C10/C8 coupling, where the C8 dimerization happens before the C10 binding (models -cf and -c) to understand how C10 interacts with C8, and finally two others, where only the FADD reaction and the C8 dimerization are taken into

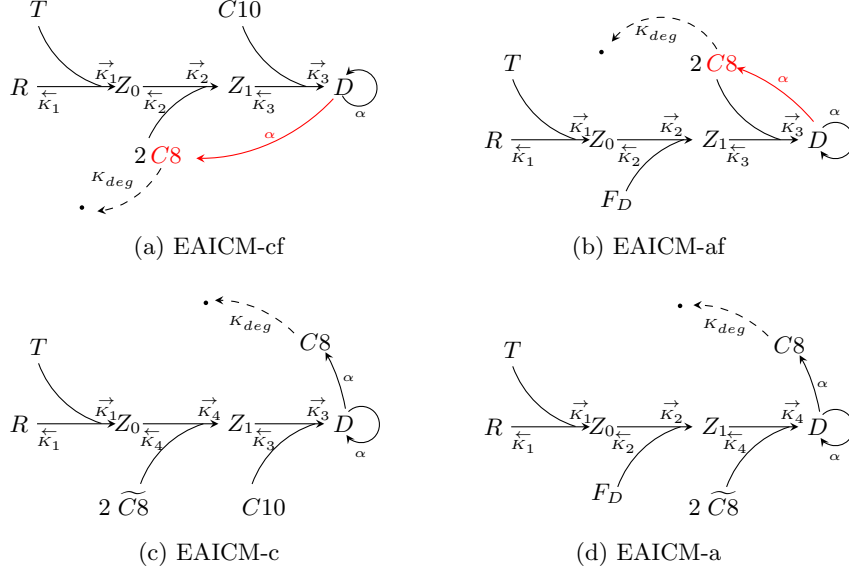


Fig. 1: Extrinsic apoptotic initiation core models (EAICM) schemes

account (models -af and -a) to examine the importance of the adaptor protein FADD, especially its regulatory capacity of pC8 recruitment.

In models without feedback loop, $\widetilde{C8}$ is a constant parameter representing available pC8.

To model the different reactions, we apply the mass-action kinetics and obtain four models of the form $dX/dt = f_{P_r}(X)$, with $f : \mathbb{R}^7 \rightarrow \mathbb{R}^7$ depending on the time-independent reaction rate vector $P_r = (\vec{K}_1, \vec{K}_1, \dots, \alpha)$, and the initial conditions:

$$\begin{cases} X_0^c = (T_0, R_0, C8_0, C10_0, Z_{0,0}, Z_{1,0}, D_0) \\ X_0^a = (T_0, R_0, C8_0, F_{D,0}, Z_{0,0}, Z_{1,0}, D_0) \end{cases}$$

EAICM-cf:

$$\begin{cases} \frac{dT}{dt} = -\vec{K}_1 TR + \vec{K}_1 Z_0, \\ \frac{dR}{dt} = -\vec{K}_1 TR + \vec{K}_1 Z_0, \\ \frac{dZ_0}{dt} = \vec{K}_1 TR - \vec{K}_1 Z_0 - \vec{K}_2 Z_0 C8^2 + \vec{K}_2 Z_1, \\ \frac{dC8}{dt} = -2\vec{K}_2 Z_0 C8^2 + 2\vec{K}_2 Z_1 + \alpha D - K_{deg} C8, \\ \frac{dZ_1}{dt} = \vec{K}_2 Z_0 C8^2 - \vec{K}_2 Z_1 - \vec{K}_3 Z_1 C10 + \vec{K}_3 D, \\ \frac{dC10}{dt} = -\vec{K}_3 C10 Z_1 + \vec{K}_3 D, \\ \frac{dD}{dt} = \vec{K}_3 Z_1 C10 - \vec{K}_3 D. \end{cases}$$

(1)

EAICM-af:

$$\begin{cases} \frac{dT}{dt} = -\vec{K}_1 TR + \vec{K}_1 Z_0, \\ \frac{dR}{dt} = -\vec{K}_1 TR + \vec{K}_1 Z_0, \\ \frac{dZ_0}{dt} = \vec{K}_1 TR - \vec{K}_1 Z_0 - \vec{K}_2 Z_0 F_D + \vec{K}_2 Z_1, \\ \frac{dF_D}{dt} = -\vec{K}_2 F_D Z_0 + \vec{K}_2 Z_1, \\ \frac{dZ_1}{dt} = \vec{K}_2 Z_0 F_D - \vec{K}_2 Z_1 - \vec{K}_3 Z_1 C8^2 + \vec{K}_3 D, \\ \frac{dC8}{dt} = -2\vec{K}_3 Z_1 C8^2 + 2\vec{K}_3 D + \alpha D - K_{deg} C8, \\ \frac{dD}{dt} = \vec{K}_3 Z_1 C8^2 - \vec{K}_3 D. \end{cases}$$

(2)

EAICM-c:

$$\left\{ \begin{array}{l} \frac{dT}{dt} = -\vec{K}_1 TR + \overleftarrow{K}_1 Z_0, \\ \frac{dR}{dt} = -\vec{K}_1 TR + \overleftarrow{K}_1 Z_0, \\ \frac{dZ_0}{dt} = \vec{K}_1 TR - \overleftarrow{K}_1 Z_0 - \vec{K}_4 Z_0 \widetilde{C8}^2 + \overleftarrow{K}_4 Z_1, \\ \frac{dC8}{dt} = \alpha D - K_{deg} C8, \\ \frac{dZ_1}{dt} = \vec{K}_4 Z_0 \widetilde{C8}^2 - \overleftarrow{K}_4 Z_1 - \vec{K}_3 Z_1 C10 + \overleftarrow{K}_3 D, \\ \frac{dC10}{dt} = -\vec{K}_3 C10 Z_1 + \overleftarrow{K}_3 D, \\ \frac{dD}{dt} = \vec{K}_3 Z_1 C10 - \overleftarrow{K}_3 D. \end{array} \right.$$

(3)

EAICM-a:

$$\left\{ \begin{array}{l} \frac{dT}{dt} = -\vec{K}_1 TR + \overleftarrow{K}_1 Z_0, \\ \frac{dR}{dt} = -\vec{K}_1 TR + \overleftarrow{K}_1 Z_0, \\ \frac{dZ_0}{dt} = \vec{K}_1 TR - \overleftarrow{K}_1 Z_0 - \vec{K}_2 Z_0 C10 + \overleftarrow{K}_2 Z_1, \\ \frac{dF_D}{dt} = -\vec{K}_2 F_D Z_0 + \overleftarrow{K}_2 Z_1, \\ \frac{dZ_1}{dt} = \vec{K}_2 F_D Z_0 - \overleftarrow{K}_2 Z_1 - \vec{K}_4 Z_1 \widetilde{C8}^2 + \overleftarrow{K}_4 D, \\ \frac{dC8}{dt} = \alpha D - K_{deg} C8, \\ \frac{dD}{dt} = \vec{K}_4 Z_1 \widetilde{C8}^2 - \overleftarrow{K}_4 D. \end{array} \right.$$

(4)

Comparing these four alternatives to experimental measurements is then necessary to investigate which of the mechanisms more faithfully reproduces the data and is capable of better generating the single-cell dynamic properties.

3 Single cell model calibration

Our models are calibrated using single cell data from Roux and al. [17]. The data measure the C8 activity before MOMP happens for 414 single cells (114 resistant and 300 sensitive) treated only with 50ng/mL of TRAIL (and not with cycloheximide contrary to [21,30]), for 10 hours. These data were obtained using the Initiator Caspase-Reporter Protein (IC-RP [21]), a FRET pair of fluorescent proteins that are linked by the peptide sequence of Bid, cleaved by C8. (FRET therefore decreases once IC-RP molecules are cleaved by C8.) In the same time, Bid is cleaved in tBid, which regulates MOMP in extrinsic apoptosis. As there is no degradation of IC-RP, contrary to tBid, it accumulates leading to the FRET stabilization at the end of the experiment for resistant cells that corresponds to the tBid degradation.

The four EAIC models are fitted to each single cell traces separately, as opposed to fitted to one averaged trace [41,42]. This approach is meant to study each single cell's heterogeneous features and it allows to obtain the parameter distribution without any assumption.

One model topology is used for both resistant and sensitive cells, since the clonal cells are genetically homogeneous. (The main differences between the two populations are attributed to the protein expression levels.)

As only data on the evolution of FRET ratio in time is available, and because the models do not take into account the FRET activation, we assume that the FRET creation corresponds only to a re-scale of C8, *ie* that the FRET dynamic is obtained from the C8 dynamic by changing the amplitude of the C8 curve and the activation time with a supplementary delay, and so the method compares directly the implemented C8 concentration to the real cleaved C8, with great attention to the slope as the FRET slope is a major indicator of the C8 activation speed.

3.1 From qualitative criteria to quantitative reference values

To evaluate and compare the four models, it is essential to define a set of criteria to determine how closely each model approaches the real data. This involves translating the main qualitative properties of the C8 curves into quantitative values that can be calculated from the model's solutions. Three fundamental properties are relevant in C8 dynamic and can be evaluated as reference values, as follows (see Figure 2):

(i) the time delay before activation of C8 is triggered; (ii) the mean slope during the C8 activation phase; and (iii) the C8 concentration reaches a stabilization value, over the last 300 minutes (especially for resistant cells). These properties can be turned into reference values by defining:

- T_{100000} evaluates the initial delay by $C8(T_{100000}) = 100000$ molecules;
- S is the C8 activation slope, as the maximum of the derivative of $C8(t)$ between 25 and 275 minutes, computed using the Matlab function *sgolayfilt*;
- V_{final} gives the final stabilization value, ie $C8(600)$, or the value of C8 at death time, for sensitive cells.

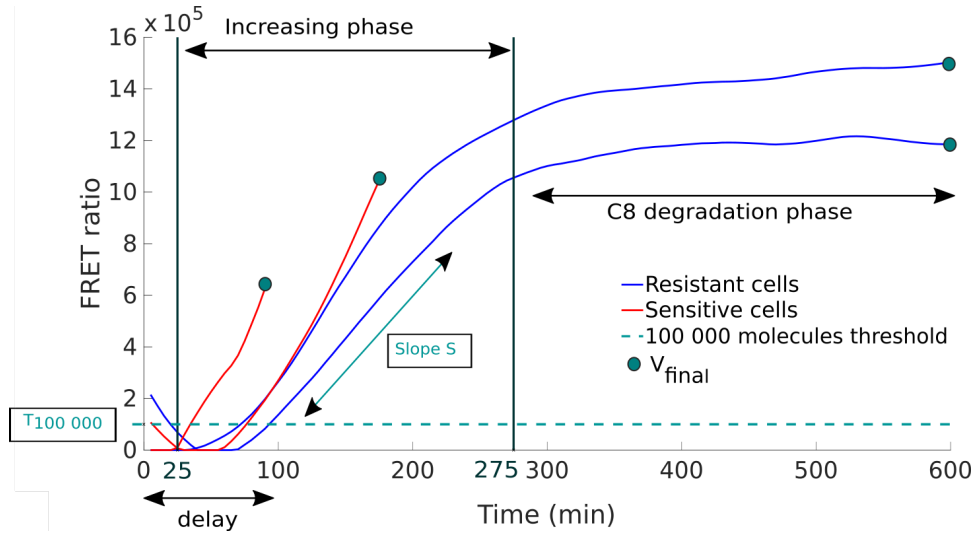


Fig. 2: Reference values and C8 features scheme

It must be noticed that the initial decreasing phase isn't taken into account. It is due to the photoactivation of the FRET and doesn't depend on the apoptosis initiation and as a result, of our models.

3.2 Distinguishing the effects of initial conditions and rate parameters on the system dynamics

Here, we use a nonlinear least-squares method to determine the parameters $P = (P_r, P_i^j, j \in \{c, a\})$ of our models $dX/dt = f_{P_r}(X)$, $P_i^j \in X_0$, where $P_r =$

$(\overleftarrow{K}_1, \overrightarrow{K}_1, \dots, K_{deg}, \alpha)$ represents the reaction rates and $P_i^c = (R_0, C8_0, C10_0)$ and $P_i^a = (R_0, C8_0, F_{D,0})$ represent the initial conditions to be evaluated during the model fit, of models EAICM-cf or EAICM-af, respectively. The other initial conditions are fixed with values from literature [21].

An euclidean norm is used to compute the cost, given by the differences between the measurements, denoted by $C8_{t_i}$, $t_i \in \mathbb{T} = \{5, 10, \dots, 600\}$ and the computed solution $C8^c$ of the chosen model taken every 5 minutes. To take into account the slope and the final C8 concentration relevance, the cost is weighted from the 25th min (approximately the beginning time of the increasing phase) until the end with heavier weight ω between the 25th and the 275th (for the slope calculated during the increasing phase). For instance, $\omega = 1000$ between min 25 and min 275. After 280 min, $\omega = 500$. Finally, denoted T_d , the cell death time, the cost \mathcal{C} is given by:

$$\mathcal{C}^2 = \sum_{t_i \in \{5, \dots, \min(20, T_d)\}} (C8_{t_i} - C8_{t_i}^c)^2 + \sum_{t_i \in \{25, \dots, \min(275, T_d)\}} \omega \times (C8_{t_i} - C8_{t_i}^c)^2 + \sum_{t_i \in \{280, \dots, \min(600, T_d)\}} \frac{\omega}{2} \times (C8_{t_i} - C8_{t_i}^c)^2. \quad (5)$$

Alternatively, for the resistant population, adding the squared slope difference between the data and the computed solution, improves the fit. For the sensitive population, we remove the last parts of the cost when the death time T_d is smaller than the first boundary of the time interval for each one of the three terms of the sum. To minimize \mathcal{C} , we used *Matlab* and its function *fminsearchbnb*, to solve an optimization problem with a physiologically significant initial guess based on the literature. To access both the individual and joint effects of reaction rate parameters and initial conditions on the dynamics, the algorithm solves three different optimization problems,

- F1. Minimize the cost \mathcal{C} with respect to both P_i and P_r ;
- F2. Fix initial conditions P_i and minimize cost \mathcal{C} with respect to P_r ;
- F3. Fix reaction constants P_r and minimize cost \mathcal{C} with respect to P_i .

Fitting only initial conditions, assumes that the model is “exact” and that the response heterogeneity comes from environmental conditions and extrinsic noise only. Conversely, fitting reaction rates only, means that the models have some variability and possibly unknown or not considered reactions or proteins impact the behaviour of C8.

It may be expected that the heterogeneity factors are a mix of the two explanations and so the fit obtained on both initial conditions and reaction rates is the best but, in this case, the results are less straightforward to interpret.

4 Analysing mechanisms for generating heterogeneity

To simulate the models, we set the initial conditions for TRAIL at $T_0 = 1500$ (from [21]), and the intermediary complexes $Z_{0,0}$, $Z_{1,0}$ and D_0 equal to 0.

Simulations are performed with *ode23* for 600 minutes with a weight $\omega = 1000$ for \mathcal{C} . For the parameter set and the other initial conditions, when they aren't estimated by the algorithm, values obtained during a first manual fit on a median real cell are used.

4.1 Comparison of the four core apoptosis models

The first point is to elucidate which of the reactions, binding of the receptor complex to F_D or to C10, best reproduces the behaviour heterogeneity of C8. To determine which of the models of type 1 or 2 best captures the extrinsic apoptosis dynamics, the norm \mathcal{C} and the reference values are computed for 114 resistant cells and 300 sensitive ones. Then, for each type of fit F1 to F3, we confront the four models by computing, for each cell and each model, the absolute value of the difference between the data slope and the C8^c slope (that is to say $|S_{EAICM,i} - S_{data,i}|$, $i \in \{1, \dots, 414\}$). Then, comparing the four results for each cell, the number of cells for which each model gives the lowest result is counted. The model with the highest score (*i.e.* the largest number of cell for which the given model gives the lowest result comparing the four models) is considered to have the best performance, as summarized in Table 1. In Appendix A, tables for the cost \mathcal{C} , the C8 final value and the delay are given.

Model Fit	fate	EAICM-cf	EAICM-c	EAICM-af	EAICM-a	Best model
F1	S. cells	120	78	57	45	EAICM-cf
	R. cells	59	11	32	12	EAICM-cf
F2	S. cells	108	79	71	42	EAICM-cf
	R. cells	75	12	26	1	EAICM-cf
F3	S. cells	269	8	20	3	EAICM-cf
	R. cells	51	23	31	9	EAICM-cf

Table 1: Number of cell best approached per model and type of fits according to the slope

Table 1 shows clearly that EAICM-cf performs better, suggesting that the caspase cluster and the feedback loop are the main mechanisms necessary to reproduce the variability in C8 slope and general cell response heterogeneity. The same results are obtained for the delay criteria. Moreover, the feedback loop seems essential to capture cell C8 dynamics, because none of the models without feedback loop accurately reproduces the three C8 properties. This result agrees with the findings of Schwarzer and al. [36] in which they demonstrate *in vivo*, the downstream inducing apoptosis effectors' effects on caspase 8. These outcomes also reveal that the clusterization of C8/C10, and so the recruitment and the activation of C8, is more important to C8 dynamics than the presence of F_D in pC8 fixation on DISC. Tummers and al. showed that caspase-8 mediates inflammasome activation independently of FADD in epithelial cells [38], further evidence that FADD isn't mandatory for caspase 8 activity. Future work would expand the study of this cluster reaction, perhaps adding more variables to take into account the effects of other proteins since the reactions around pC8 recruitment (especially its interactions with pC10 and c-FLIP) are still unclear.

Another hypothesis could also be made in this case, assuming that in EAICM-cf, the F_D action is not present in the equations but indeed taken into account since C8 is still recruited at the DISC level.

4.2 The feedback loop mechanism

The second question to address in this Section concerns the effects of the positive feedback loop on C8 to understand its importance on C8 dynamics.

To evaluate the feedback loop impacts on the C8 dynamic, we use the parameters obtained from fit F1, on both initial conditions and reaction rates. Figure 3 and Figure 4 (a) and (c) compare the FRET ratio and the $C8^c$ curve corresponding to the models 1 with and without feedback for selected resistant and sensitive cells from the cell populations in [17]. It seems clear that the model without feedback fails to reproduce the initial delay before C8 activation. In a second plot, Figure 3 and Figure 4 (b) and (d) compare the relative weights of the different terms that contribute to C8 activation. This is a method developed by Casagrande and al. in [34] and consists in representing the absolute values curve of each term that composes the C8 equation, divided by the sum of all absolute values, to normalize. For instance, if we consider the following C8 equation of EAICM-cf:

$$\frac{dC8}{dt} = -2\vec{K}_2 Z_0 C8^2 + 2\overleftarrow{K}_2 Z_1 + \alpha D - K_{deg} C8, \quad (6)$$

then the plotted curves are:

$$\left\{ \begin{array}{l} \frac{|K_{deg} C8|}{|K_{deg} C8| + |\alpha D| + |2\overleftarrow{K}_2 Z_1| + |2\vec{K}_2 Z_0 C8^2|}, \\ \frac{|\alpha D|}{|K_{deg} C8| + |\alpha D| + |2\overleftarrow{K}_2 Z_1| + |2\vec{K}_2 Z_0 C8^2|}, \\ \frac{|2\overleftarrow{K}_2 Z_1|}{|K_{deg} C8| + |\alpha D| + |2\overleftarrow{K}_2 Z_1| + |2\vec{K}_2 Z_0 C8^2|}, \\ \frac{|2\vec{K}_2 Z_0 C8^2|}{|K_{deg} C8| + |\alpha D| + |2\overleftarrow{K}_2 Z_1| + |2\vec{K}_2 Z_0 C8^2|}. \end{array} \right. \quad (7)$$

Similar plots for the EAICM-af and EAICM-a models can be found in Appendix B. First, comparing Figure 3 and Figure 4, notice that there are essentially no differences between resistant and non resistant cells in the component-wise analysis. However, there is no activation delay in C8 curve for the models without a feedback loop. Then, focusing on the $|\alpha D|$ variation (corresponding to the feedback loop effect), one can observe that $|\alpha D|$ reaches its maximum and $|K_{deg} C8|$ its minimum at approximately the same moment, which also coincides with the moment when C8 starts increasing. Recall that αD drives all the effective caspase cascade and the feedback loop, so the coincidence between maximum of αD and beginning of C8 activation suggests that the feedback loop markedly increases the production of C8. Finally, observe that, in the absence

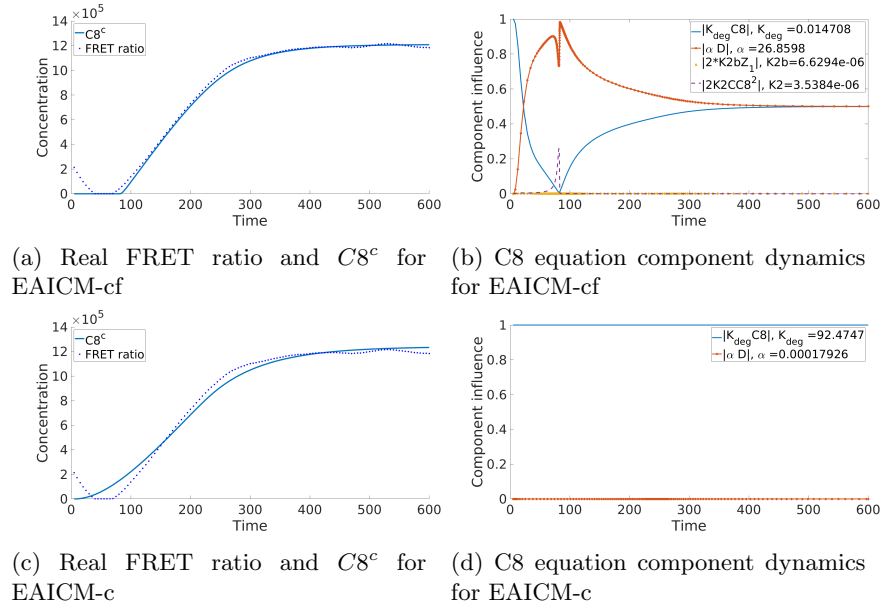


Fig. 3: Comparison of C8 dynamics and main properties for models EAICM-cf (a),(b) and EAICM-c (c),(d), for the resistant cell n. 10

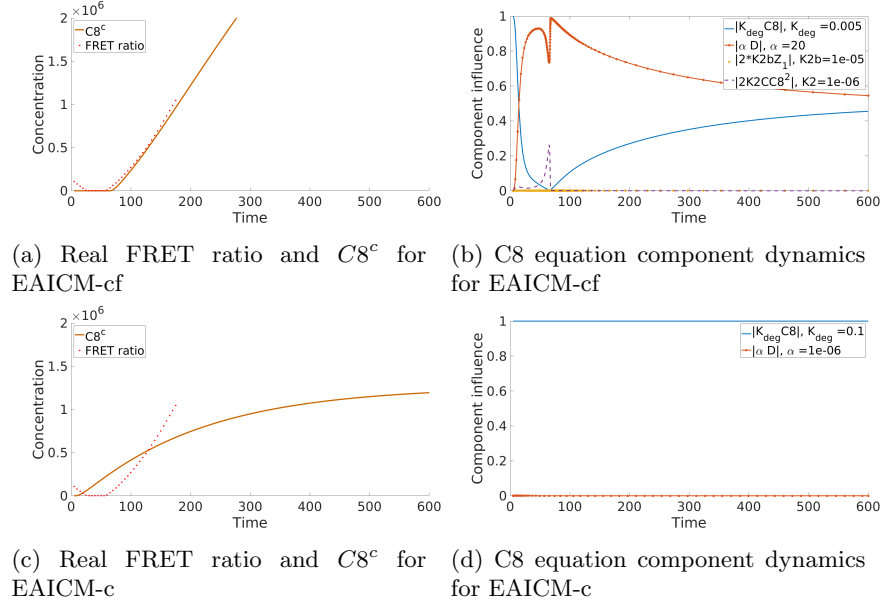


Fig. 4: Comparison of C8 dynamics and main properties for models EAICM-cf (a),(b) and EAICM-c (c),(d) for the sensitive cell n. 121 - *simulations were performed for 600 min for comparison needs*

of feedback loop, the term $|K_{deg}C8|$ is responsible for all the dynamics of C8, inducing similar activation slopes for the two phenotypes.

Overall, the feedback loop helps to refine cell decision, by improving modulation of the activation slope, as illustrated by the term αD : for the sensitive cell, in the first 50 minutes αD increases in a much steeper manner. The feedback represents a supplementary set of regulatory mechanisms that is surely independent from the complex TRAIL/receptors and possibly downstream, yet with a decisive impact on C8 activation.

The next step is evaluating the effect of variability in initial conditions on both C8 and cell fate.

4.3 Initial conditions impacts on slope values

This section analyses the initial conditions distributions and compares them with our reference values, to identify some mathematical patterns that can help predicting the cell fate. The goal is to find those distributions for which the resistant and sensitive phenotypes present a significant difference, or a link between the initial conditions and C8 dynamics.

To represent the data obtained after model's fitting, the bar chart of the cell density after model fitting according to their parameter distribution and the scatter plot of the initial condition distribution in logscale according to our reference values (for example, the slope) are used. For each type of graph, resistant and sensitive cells are differentiated to find specific behaviours.

The parameters used for comparison are those obtained from fit F3 (only on the initial conditions), to evaluate the environmental impacts. A clear difference for $C10_0$ between resistant and sensitive cells is observed on the logscale scatter plots in Figure 5, with a linear correlation between the slope and the initial protein value with highly clustered points for the two types of cells. This is also the case for the F_D distribution that can be found in Figure 10. To understand how

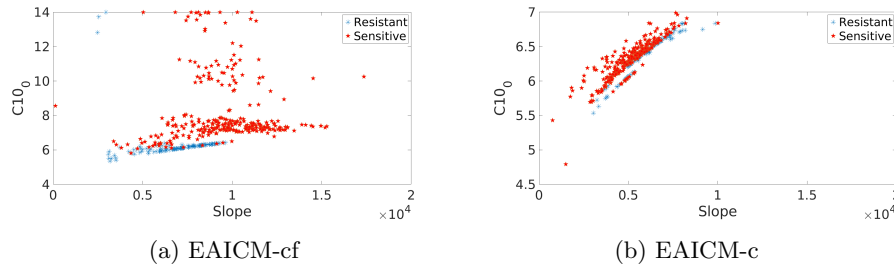


Fig. 5: Scatter plot of $C10_0$ values according to the slope, depending on cell fate, for the EAICM-cf and EAICM-c

these two initial conditions, as well as R_0 variation, affect the C8 dynamics, Figure 6 shows the evolution of the $C8^c$ curves for each model, as two of the initial conditions are fixed and the third is given by the median value obtained with the

fit on all the parameters for resistant cells (given in appendix D, in black dash dots on Figure 6) multiplied by $m \in \{0, 0.2, 0.4, 0.6, 0.8, 1.2, 1.4, 1.6, 1.8, 2, 4, 10\}$.

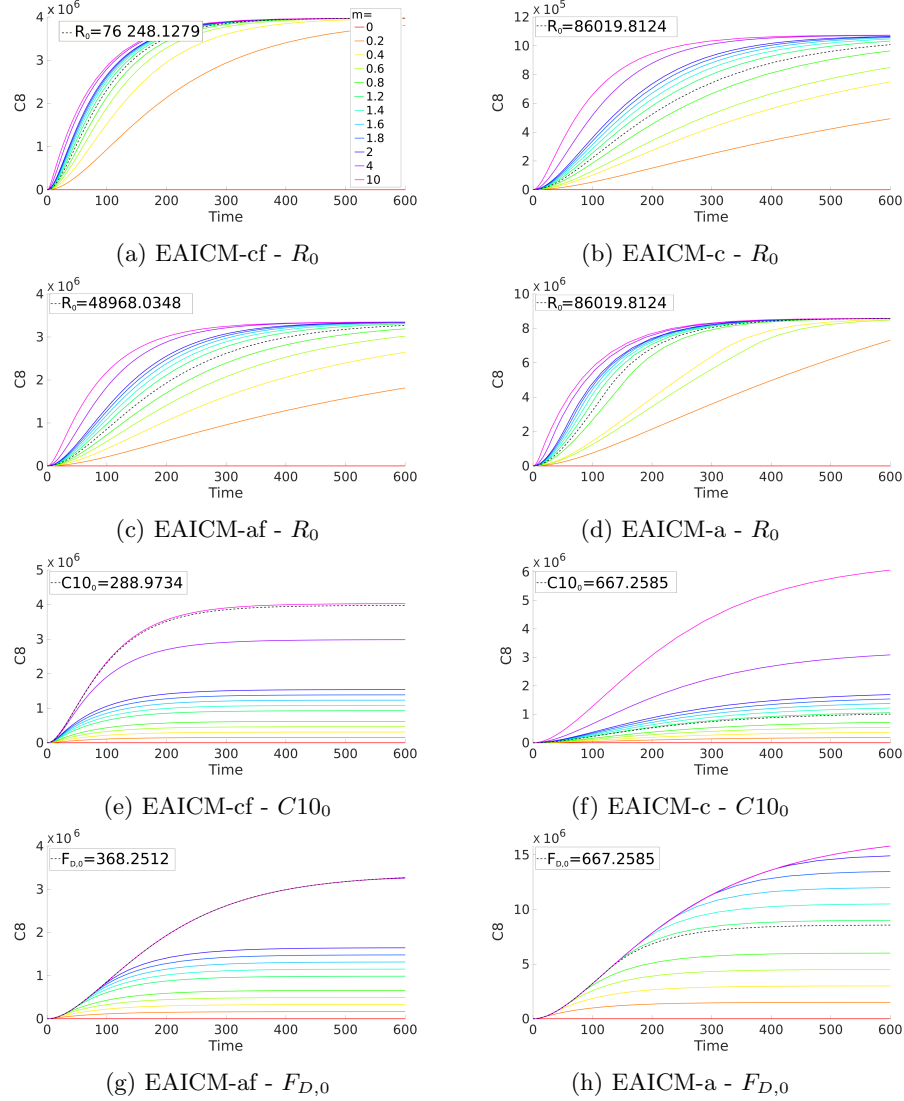


Fig. 6: Initial condition variation effects on C8 dynamic. The estimated parameters P_i are indicated at the top left corners and used as reference values to vary the initial condition, in the range $[0, 10X_0]$, where $X_0 = R_0$ in (a)-(d); $X_0 = C10_0$ in (e)-(f); and $X_0 = F_{D,0}$ in (g)-(h).

First of all, observe that an increase in the receptor number enhances the slope of C8 and so it speeds up the C8 production and delays the C8 degrada-

tion since the stabilization happens later but it doesn't influence the total C8 production (C8 stabilization at the same value). Hence, R_0 is likely to contribute to determination of the C8 activation threshold.

A saturation effect is observed in every model, for the recruited C8, that can't exceed a certain threshold in the total C8 production. This is in agreement with single cell traces since, independently of the TRAIL dose, even at saturated concentration with all the receptors occupied, not every cell commits to apoptosis. An improvement in our models may be necessary to take into account the necessary receptors trimerization that leads to DISC formation [16].

Another observation is that larger $C10_0$ induce larger values for C8 stabilization. An increase in $C10_0$ enhances the C8 production speed but doesn't impact the degradation beginning time. Observe that $C10_0$ also plays a significant role in feedback loop-free models. This effect of $C10_0$ on C8 behaviour confirms the essential role of caspase cluster to trigger cell-death, as shown in Dickens and al. [16].

Finally, increasing $F_{D,0}$ delays C8 degradation and improves C8 production or recruitment, but doesn't speed up the C8 production since the activation slope doesn't show much variation. Furthermore, increasing $F_{D,0}$ leads to an increase in C8, thus making it possible to exceed the C8 threshold responsible for cell death and confirming that FADD is necessary to trigger the extrinsic cell death as demonstrated by Kuang and al. in [18]. Similarly to $C10_0$, F_D also has more influence on the model without feedback loop, suggesting that the feedback loop has a saturation effect on C8 dynamic.

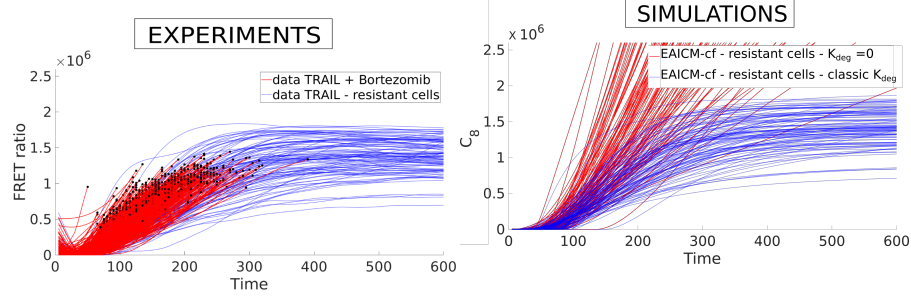
4.4 Model validation and degradation specificity

Comparison of the reaction rates distributions, singles out C8 degradation rate which exhibits a large discrepancy between resistant and sensitive populations, with values related by a factor $K_{deg}^r \approx 10K_{deg}^s$.

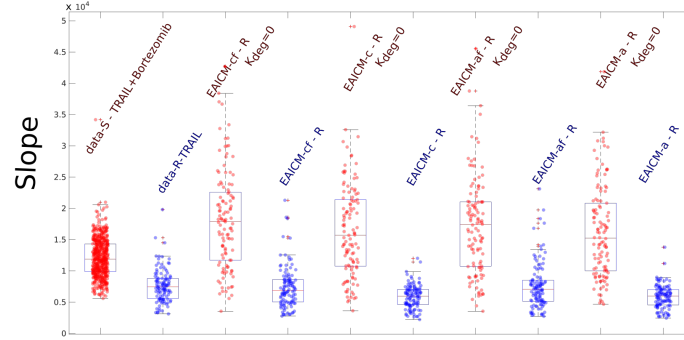
As seen in Section 4.2, degradation is the process that counteracts C8 activation and, when the term $K_{deg}C8$ becomes sufficiently high, the stabilization phase sets in. Decreasing the degradation rate constant should lead to higher activation slopes and effectively "switch" cells from the resistant to the sensitive populations.

Data from [17] includes a second group of 563 cells treated with 50ng/mL of TRAIL and 100ng/mL of Bortezomib, a proteasome inhibitor drug that blocks C8 degradation and drives the cell to commit apoptosis. To validate our models, our hypothesis is that, setting K_{deg} to zero in model EAICM-cf (while keeping other parameters as estimated for each resistant cell), will elicit the same response as Bortezomib, thus transforming the resistant population into sensitive. Figure 7(a) shows the FRET ratio of the two groups of cells: the resistant population of 100 cells treated only with TRAIL and the second group of 563 cells treated with TRAIL and Bortezomib. These experimental results are to be compared with Figure 7(b), that represents the C8^c EAICM-cf model curves for our

original resistant population, with all the corresponding estimated parameters except for K_{deg} , which is set to 0.



(a) Comparison of FRET ratio between resistant cells treated only with TRAIL and cells treated with TRAIL and Bortezomib. (b) Comparison of $C8^c$ from EAICM-cf for resistant cells treated only with TRAIL, with $K_{deg} = 0$ and with classic degradation.



(c) Slope distribution according to the model used and the C8 degradation rate.

Fig. 7: Degradation study

Observe that the model predictions in Figure 7(b) and (c) are quite similar to the experimental data. Figure 7

shows that, imposing a null degradation for our model, allows to reproduce a large heterogeneity range and the main features (delay and bigger slope) of C8 dynamic of the population treated with Bortezomib, thus validating our hypothesis.

Why does the sensitive population of the first group of cells show a markedly lower K_{deg} constant? Perhaps a (negative) feedback or similar mechanism is also acting on the degradation process, annulling its effect in the case of a steep C8 activation. However, it might be the case that the estimation of K_{deg} among the sensitive population is not fully reliable: indeed, recall that the degradation term is linear, $K_{deg}C8$, and that active caspase 8 is absent at the beginning

($C8(0) = 0$), implying a very low degradation when compared to terms of the form $K_2 Z_1$ or αD which are proportional to $T_0 R_0$. In addition, sensitive cells die relatively early during the first 150 minutes, so that there are much fewer measurement points available than for resistant cells. New modeling steps are needed to further study the C8 degradation process.

5 Discussion and Conclusion

This paper studies the role and the relevance of several components of the extrinsic apoptosis initiation pathway in cell response heterogeneity. Four minimal ODE models are proposed, taking into account the major steps of the extrinsic pathway: the TRAIL/receptors association, the DISC formation with the recruitment of pro-caspase 8 and, either a focus on the FADD action, or a particular attention to the cluster formation of pC8 and pC10. These models also represent the C8 activation with (or without) a positive feedback loop on C8 to integrate a supplementary regulation of C8 downstream. Finally, as cell decision to commit apoptosis seems to happen before effective caspase activation and MOMP, all the downstream apoptosis steps were combined in a single variable.

The models were calibrated to single cell data from a cloned population treated with death ligand TRAIL. The corresponding initial conditions and/or parameters were analysed to search for correlations between molecular factors and/or network interactions, and the resulting cell fates.

Our analysis selects two mechanisms that significantly contribute to cell response heterogeneity: the clusterization of the caspases C8/C10 and subsequent C8 activation and, to a larger extent, the positive feedback loop. The formation of C8/C10 clusters accelerates C8 activation by increasing C8 production as well as the slope of the curve (see the effect of $C10_0$), while the F_D reaction does not greatly affect the slope but delays the stabilization time. Therefore, caspase clusterization has a greater capacity to generate variability in cell response.

The positive feedback is important in the timing of C8 dynamics, particularly in reproducing the initial delay observed in C8 activation. Studying the components of the C8 equation shows that activation of C8 is triggered when the feedback loop has a maximum effect on C8 and degradation is still negligible. Conversely, when the degradation and the feedback loop terms reach similar levels C8 leaves the high slope phase, revealing that the balance between feedback loop and C8 degradation plays a major role in cell fate.

Another role of the feedback loop is to introduce a saturation on the maximum level of C8 induced by variability in initial conditions: indeed, for our two models with positive feedback, increasing the initial numbers of molecules leads to an increase in the maximum C8 levels, but this maximum value has an upperbound independent of the initial numbers. This reveals a large robustness of the feedback models with respect to variations in initial amounts of molecules.

Finally, our models faithfully reproduce the experiments involving Bortezomib, a drug that blocks C8 degradation. In our models, application of Bortezomib is represented by setting $K_{deg} = 0$, and the corresponding effect is to

increase all activation slopes into the range observed for the sensitive population. Based on the mechanisms and interactions selected by our methods, future work includes the development of a more detailed model to answer further questions such as the need for trimerization of the death receptor, understand the process of caspase degradation during the first hours of C8 activation, or adding new variables to investigate the impact of the anti-apoptotic component c-FLIP.

References

1. Matveeva, A., Fichtner, M., McAllister, K., McCann, C., Sturrock, M., Longley, D. B. and Prehn, J. H. M.: Heterogeneous responses to low level death receptor activation are explained by random molecular assembly of the Caspase-8 activation platform. In *PLoS computational biology*, vol. 15, n. 9, p. e1007374. Public Library of Science, San Francisco, CA USA (2019)
2. Bouralexis, S., Findlay, D. M. and Evdokiou, A.: Death to the bad guys: targeting cancer via Apo2L/TRAIL. In *Apoptosis*, vol. 10, n. 1, p. 35–51. Springer (2005)
3. Shlyakhtina, Y., Pavet, V. and Gronemeyer, H.: Dual role of DR5 in death and survival signaling leads to TRAIL resistance in cancer cells. In *Cell death & disease*, vol. 8, n. 8, p. e3025. Nature Publishing Group (2017)
4. Eskes, R., Desagher, S., Antonsson, B., Martinou, J. C.: Bid induces the oligomerization and insertion of Bax into the outer mitochondrial membrane. In *Molecular and cellular biology*, vol. 20, n. 3, p. 929–935. Am Soc Microbiol (2000)
5. Fricker, N., Beaudouin, J., Richter, P., Eils, R., Krammer, P. H. and Lavrik, I. N.: Model-based dissection of CD95 signaling dynamics reveals both a pro- and antiapoptotic role of c-FLIP. In *The Journal of cell biology*, vol. 190, n. 3, p. 377–389. Rockefeller University Press (2010)
6. Han, L., Zhao, Y., and Jia, X.: Mathematical modeling identified c-FLIP as an apoptotic switch in death receptor induced apoptosis. In *Apoptosis*, vol. 13 n. 10, p. 1198–1204. Springer (2008)
7. Tsuchiya, Y., Nakabayashi, O. and Nakano, H.: FLIP the Switch: Regulation of Apoptosis and Necroptosis by cFLIP. In *International journal of molecular sciences*, vol. 16, n. 12, p. 30321–30341. Multidisciplinary Digital Publishing Institute (2015)
8. Hughes, M. A., Powley, I. R., Jukes-Jones, R., Horn, S., Feoktistova, M., Fairall, L., Schwabe, J. W. R., Leverkus, M., Cain, K. and MacFarlane, M.: Co-operative and hierarchical binding of c-FLIP and caspase-8: a unified model defines how c-FLIP isoforms differentially control cell fate. In *Molecular cell*, vol. 61, n. 6, p. 834–849. Elsevier (2016)
9. Hillert, L. K., Ivanisenko, N. V., Espe, J., König, C., Ivanisenko, V. A., Kähne, T. and Lavrik, I. N.: Long and short isoforms of c-FLIP act as control checkpoints of DED filament assembly. In *Oncogene*, vol. 39, n. 8, p. 1756–1772. Nature Publishing Group (2020)
10. Horn, S. and Hughes, M. A., Schilling, R., Sticht, C., Tenev, T., Ploesser, M., Meier, P., Sprick, M. R., MacFarlane, M. and Leverkus, M.: Caspase-10 negatively regulates caspase-8-mediated cell death, switching the response to CD95L in favor of NF- κ B activation and cell survival. In *Cell reports*, vol. 19, n. 4, p. 785–797. Elsevier (2017)
11. Wang, Jin and Chun, Hyung J and Wong, Wilson and Spencer, David M and Lenardo, Michael J: Caspase-10 is an initiator caspase in death receptor signaling. In *Proceedings of the National Academy of Sciences*, vol. 98, n. 24, p. 13884–13888, National Acad Sciences (2001)

12. Wachmann, Katherine and Pop, Cristina and van Raam, Bram J and Drag, Marcin and Mace, Peter D and Snipas, Scott J and Zmasek, Christian and Schwarzenbacher, Robert and Salvesen, Guy S and Riedl, Stefan J: Activation and specificity of human caspase-10. In *Biochemistry*, vol. 49, n. 38, p. 8307–8315, ACS Publications (2010)
13. Kischkel, Frank C and Lawrence, David A and Tinel, Antoine and LeBlanc, Heidi and Virmani, Arvind and Schow, Peter and Gazdar, Adi and Blenis, John and Arnott, David and Ashkenazi, Avi: Death receptor recruitment of endogenous caspase-10 and apoptosis initiation in the absence of caspase-8. In *Journal of Biological Chemistry*, vol. 276, n. 49, p. 46639–46646, ASBMB (2001)
14. Raulf, N and El-Attar, R and Kulms, D and Lecis, D and Delia, D and Walczak, H and Papenfuss, K and Odell, E and Tavassoli, M: Differential response of head and neck cancer cell lines to TRAIL or Smac mimetics is associated with the cellular levels and activity of caspase-8 and caspase-10. In *British journal of cancer*, vol. 111, n. 10, p. 1955–1964, Nature Publishing Group (2014)
15. Kumari, Rajni and Deshmukh, Ruhi S and Das, Sanjeev: Caspase-10 inhibits ATP-citrate lyase-mediated metabolic and epigenetic reprogramming to suppress tumorigenesis. In *Nature communications*, vol. 10, n. 1, p. 1–15, Nature Publishing Group (2019)
16. Dickens, L. S., Boyd, R. S. and Jukes-Jones, R., Hughes, M. A., Robinson, G. L., Fairall, L., Schwabe, J. WR., Cain, Kelvin and MacFarlane, Marion : A death effector domain chain DISC model reveals a crucial role for caspase-8 chain assembly in mediating apoptotic cell death. In *Molecular cell*, vol.47, n. 2, p. 291–305 . Elsevier (2012)
17. Roux, J., Hafner, M., Bandara, S., Sims, J. J., Hudson, H., Chai, D. and Sorger, P. K. : Fractional killing arises from cell-to-cell variability in overcoming a caspase activity threshold. In *Molecular systems biology*, vol. 11, n. 5. John Wiley & Sons, Ltd (2015)
18. Kuang, A.A., Diehl, G. E., Zhang, J. and Winoto, Astar : FADD is required for DR4-and DR5-mediated apoptosis LACK of TRAIL-induced apoptosis in FADD-deficient mouse embryonic fibroblasts. In *Journal of Biological Chemistry*, vol. 275, n. 33, p.25065–25068. ASBMB (2000)
19. Chang, D. W., Xing, Z., Capacio, V. L., Peter, M. E. and Yang, X. : Interdimer processing mechanism of procaspase-8 activation. In *The EMBO journal*, vol.22, n. 16, p. 4132–4142. John Wiley & Sons, Ltd (2003)
20. Schleich, K and Buchbinder, JH and Pietkiewicz, S and Kähne, T and Warnken, U and Öztürk, S., Schnölzer, M., Naumann, M., Krammer, P. H. and Lavrik, IN. : Molecular architecture of the DED chains at the DISC: regulation of procaspase-8 activation by short DED proteins c-FLIP and procaspase-8 prodomain. In *Cell death and differentiation*, vol. 23, n. 4, p. 681. Nature Publishing Group (2016)
21. Albeck, J. G., Burke, J. M., Spencer, S. L., Lauffenburger, D. A. and Sorger, P. K. : Modeling a snap-action, variable-delay switch controlling extrinsic cell death. In *PLoS biology*, vol.6, n. 12, p. e299. Public Library of Science (2008)
22. Lederman, E. E.Hope, J. M. and King, M. R. : Mass Action Kinetic Model of Apoptosis by TRAIL-Functionalized Leukocytes. In *Frontiers in oncology*, vol. 8. Frontiers Media SA (2018)
23. Bertaux, F., Stoma, S., Drasdo, D. and Batt, G. : Modeling dynamics of cell-to-cell variability in TRAIL-induced apoptosis explains fractional killing and predicts reversible resistance. In *PLoS computational biology*, vol. 10, n. 10, p. e1003893. Public Library of Science (2014)

24. Chong, K. H., Samarasinghe, S., Kulasiri, D. and Zheng, J. : Mathematical modelling of core regulatory mechanism in p53 protein that activates apoptotic switch. In *Journal of theoretical biology*, vol. 462, p. 134–147. Elsevier (2019)
25. Ballweg, R., Paek, A. L. and Zhang, T.: A dynamical framework for complex fractional killing. In *Scientific reports*, vol.7, n. 1, p. 8002. Nature Publishing Group (2017)
26. Buchbinder, J. H., Pischel, D., Sundmacher, K., Flassig, R. J. and Lavrik, I. N. : Quantitative single cell analysis uncovers the life/death decision in CD95 network. In *PLoS computational biology*, vol. 14, n. 9, p. e1006368. Public Library of Science (2018)
27. Bentele, M., Lavrik, I., Ulrich, M., Stösser, S., Heermann, DW., Kalthoff, H., Krammer, P. H. and Eils, R.: Mathematical modeling reveals threshold mechanism in CD95-induced apoptosis. In *J Cell Biol*, vol. 166, n. 6, p. 839–851. Rockefeller University Press (2004)
28. Neumann, L., Pforr, C., Beaudouin, J., Pappa, A., Fricker, N., Krammer, P. H., Lavrik, I. N. and Eils, R. : Dynamics within the CD95 death-inducing signaling complex decide life and death of cells. In *Molecular systems biology*, vol. 6, n.1. John Wiley & Sons, Ltd (2010)
29. Paek, A. L., Liu, J. C., Loewer, A., Forrester, W.C. and Lahav, G. : Cell-to-cell variation in p53 dynamics leads to fractional killing. In *Cell*, vol. 165, n. 3, p. 631–642. Elsevier (2016)
30. Rehm, M., Huber, H. J., Dussmann, H. and Prehn, J. HM. : Systems analysis of effector caspase activation and its control by X-linked inhibitor of apoptosis protein. In *The EMBO journal*, vol.25, n. 18, p. 4338–4349. John Wiley & Sons, Ltd (2006)
31. Martin D. A. Siegel, R. M., Zheng, L. and Lenardo, M. J. : Membrane oligomerization and cleavage activates the caspase-8 (FLICE/MACH α 1) death signal. In *Journal of Biological Chemistry*, v. 273, n. 8, p. 4345–4349. ASBMB (1998)
32. Fallahi-Sichani, M., Honarnejad, S., Heiser, L. M., Gray, J.W. and Sorger, P. K. : Metrics other than potency reveal systematic variation in responses to cancer drugs. In *Nature chemical biology*, v. 9, n. 11, p. 708. Nature Publishing Group (2013)
33. Flusberg, D. A., Roux, J. and Spencer, S. L., and Sorger, P. K. : Cells surviving fractional killing by TRAIL exhibit transient but sustainable resistance and inflammatory phenotypes. In *Molecular biology of the cell*, vol. 24, n. 14, p. 2186–2200. Am Soc Cell Biol (2013)
34. Casagrande, S., Touzeau, S., Ropers, D. and Gouzé, JL. : Principal process analysis of biological models. In *BMC systems biology*, vol. 12, n.1, p. 68. Springer (2018)
35. Hillert, L. K and Ivanisenko, N. V , Busse, D. , Espe, J. , König, C. , Peltek, S. E , Kolchanov, N. A ,Ivanisenko, V. A and Lavrik, Inna N : Dissecting DISC regulation via pharmacological targeting of caspase-8/c-FLIP L heterodimer. In *Cell Death & Differentiation*. p.1-14, Nature Publishing Group (2020)
36. Schwarzer, R., Jiao, H., Wachsmuth, L. Tresch, A. and Pasparakis, M. :FADD and Caspase-8 Regulate Gut Homeostasis and Inflammation by Controlling MLKL-and GSDMD-Mediated Death of Intestinal Epithelial Cells. In *Immunity*, Elsevier(2020)
37. Strasser, Andreas and Vaux, David L : Cell Death in the Origin and Treatment of Cancer. In *Molecular Cell*, Elsevier(2020)
38. Tummers, Bart and Mari, Luigi and Guy, Clifford S and Heckmann, Bradlee L and Rodriguez, Diego A and Rühl, Sebastian and Moretti, Julien and Crawford, Jeremy Chase and Fitzgerald, Patrick and Kanneganti, Thirumala-Devi and others : Caspase-8-Dependent Inflammatory Responses Are Controlled by Its Adaptor, FADD, and Necroptosis. In *Immunity*, Elsevier (2020)

39. Amaral, Marcelo Pires and Bortoluci, Karina Ramalho : Caspase-8 and FADD: Where Cell Death and Inflammation Collide. In *Immunity*, vol. 52, n. 6, p.890–892, Elsevier(2020)
40. Chaudhry, M Zeeshan and Casalegno-Garduno, Rosaely and Sitnik, Katarzyna M and Kasmapiour, Bahram and Pulm, Ann-Kathrin and Brizic, Ilija and Eiz-Vesper, Britta and Moosmann, Andreas and Jonjic, Stipan and Mocarski, Edward S and others : Cytomegalovirus inhibition of extrinsic apoptosis determines fitness and resistance to cytotoxic CD8 T cells. In *Proceedings of the National Academy of Sciences*, vol. 117, n.23, p.12961–12968, National Acad Sciences (2020)
41. Llamasi, Art  mis and Gonzalez-Vargas, Andres M and Versari, Cristian and Cinquemani, Eugenio and Ferrari-Trecate, Giancarlo and Hersen, Pascal and Batt, Gregory : What population reveals about individual cell identity: single-cell parameter estimation of models of gene expression in yeast. In *PLoS computational biology*, vol.12, n.2, p.e1004706, Public Library of Science San Francisco, CA USA (2016)
42. Pereira, Luis Carlos Gomes : Thesis : Modeling cell response heterogeneity to proapoptotic ligands. COMUE Universit   C  te d’Azur (2015-2019)

Appendices

A Comparison models tables

Fit \ Model	fate	EAICM-cf	EAICM-c	EAICM-af	EAICM-a	Best model
F1	S. cells	177	20	95	8	EAICM-cf
	R. cells	51	3	52	8	EAICM-cf/EAICM-af
F2	S. cells	0	20	0	280	EAICM-a
	R. cells	0	102	0	12	EAICM-c
F3	S. cells	0	63	1	236	EAICM-a
	R. cells	2	95	0	17	EAICM-c

Table 2: Number of cell best approached per model and type of fits, comparing \mathcal{C} value

Fit \ Model	fate	EAICM-cf	EAICM-c	EAICM-af	EAICM-a	Best model
F1	S. cells	132	98	20	50	EAICM-cf
	R. cells	46	43	9	16	EAICM-cf
F2	S. cells	130	103	8	59	EAICM-cf
	R. cells	55	48	1	10	EAICM-cf
F3	S. cells	222	20	17	41	EAICM-cf
	R. cells	64	10	33	7	EAICM-cf

Table 3: Number of cell best approached per model and type of fits comparing the delay, ie $|T_{100000,EAICM,i} - T_{100000,data,i}|$, $i \in \{1, \dots, 414\}$

Model \ Fit	fate	EAICM-cf	EAICM-c	EAICM-af	EAICM-a	Best model
F1	S. cells	91	108	46	55	EAICM-c
	R. cells	45	16	35	18	EAICM-cf
F2	S. cells	68	111	59	62	EAICM-c
	R. cells	51	10	44	9	EAICM-cf
F3	S. cells	263	0	23	14	EAICM-cf
	R. cells	9	26	62	17	EAICM-af

Table 4: Number of cell best approached per model and type of fits according to C8 final value, ie comparing $|V_{final,EAICM,i} - V_{final,data,i}|$, $i \in \{1, \dots, 414\}$

B Feedback loop effects for EAICM-af and EAICM-a

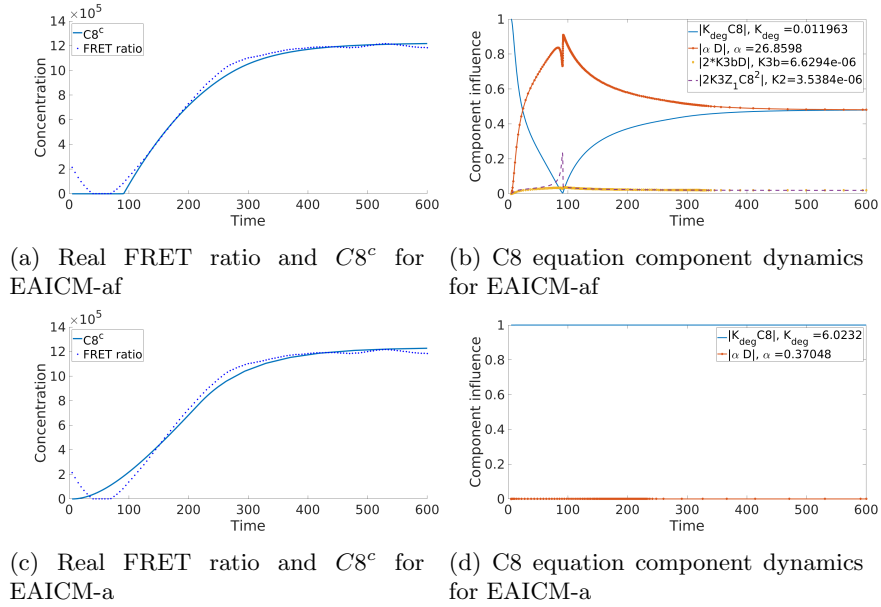
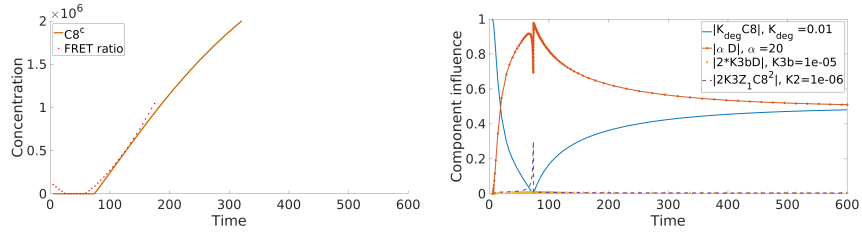
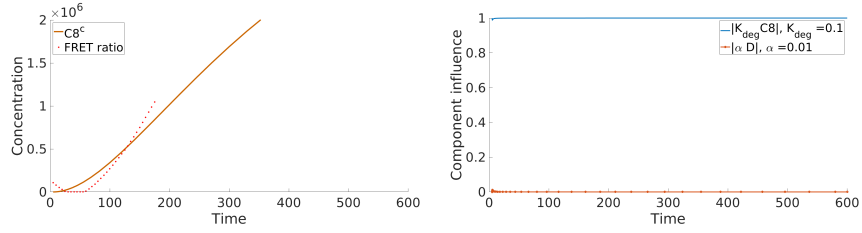


Fig. 8: Comparison of C8 main features with the dynamic of each C8 equation component of EAICM-af (a),(b) and EAICM-a (c),(d) for the resistant cell n. 10



(a) Real FRET ratio and $C8^c$ for EAICM-af (b) C8 equation component dynamics for EAICM-af



(c) Real FRET ratio and $C8^c$ for EAICM-a (d) C8 equation component dynamics for EAICM-a

Fig. 9: Comparison of C8 main features with the dynamic of each C8 equation component of EAICM-af (a),(b) and EAICM-a (c),(d) for the sensitive cell n. 121 - simulations were performed for 600 min for comparison needs

C Initial condition and cell fate correlations for EAICM-af

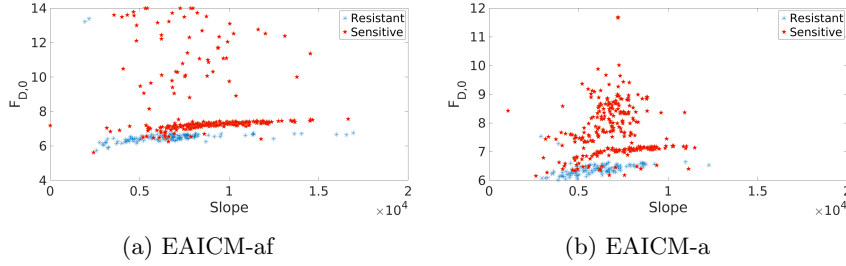


Fig. 10: Scatter plot of $F_{D,0}$ values according to the slope, depending on the cell fate for EAICM-af and EAICM-a

D Median parameter values from the fit on both initial conditions and reaction rates used in Figure 6

	EAICM-cf		EAICM-c		EAICM-af		EAICM-a	
	R. cells	S. cells	R. cells	S. cells	R. cells	S. cells	R. cells	S. cells
\vec{K}_1	4.3955e-07	2.7388e-07	6.5892e-08	1.2254e-07	1.6320e-07	4.0018e-07	6.5892e-08	1.2254e-07
\overleftarrow{K}_1	0.0052	0.01129	1.1176	1.7906	3.4358e-04	0.0011	1.1177	1.7907
\vec{K}_2	1.5590e-05	2.4304e-05			0.0525	0.0649	25.5081	14.8725
\overleftarrow{K}_2	2.9114e-04	9.6920e-04			3.6929e-06	1.2142e-05	2.3934	2.1489
\vec{K}_3	0.0012	0.002792	0.002045	0.002206	4.5915e-05	2.1800e-04		
\overleftarrow{K}_3	0.0273	0.1607	20.1550	26.9179	2.0294	9.2971		
\vec{K}_4			16.5523	25.6951			16.5524	25.6952
\overleftarrow{K}_4			2.6201	2.6749			2.6202	2.6750
K_{deg}	0.0133	0.004012	0.0001165	0.001765	0.0122	0.0108	0.0117	0.0018
α	36.2215	48.8287	1.3188	279.2583	27.3338	76.6511	131.8895	279.2584
R_0	7.6248e+04	6.7850e+04	8.6019e+04	4.0387e+04	4.8968e+04	5.6593e+04	8.6020e+04	4.0388e+04
$C_{8,0}$	288.9734	905.9665	667.2585	337.2630	368.2512	663.5847	667.2585	337.2631
$C_{10,0}$	2.2325e+03	3.1050e+04	761.9486	1.0829e+04				
$F_{D,0}$					2.9291e+03	5.3681e+04	761.9486	1.0830e+04

Table 5: Median reaction rates and initial conditions for all models determined with the fit on both initial conditions and reactions rates

E Operation of the parameter model and reference value tables

In addition of this article,, we provide all the parameters tables and the reference values tables obtained with our 3 types of fit for the 414 cells treated with TRAIL only. A line corresponds to one parameter in that order (C , \vec{K}_1 , \overleftarrow{K}_1 , \vec{K}_2 , \overleftarrow{K}_2 , \vec{K}_3 , \overleftarrow{K}_3 , \vec{K}_4 , \overleftarrow{K}_4 , α , K_{deg} , R_0 , $C_{8,0}$, $C_{10,0}$

or $F_{D,0}$) and without \vec{K}_4 and \overleftarrow{K}_4 for models with feedback loop.

Parameters_EAICM-cf_NON_resist_fit_Pr_only.mat	} 12×300 table that gives the 8 reactions rates (10 for models without feedback loop) in the first lines and the 3 initial conditions obtained from the fit only on reaction rates for the 300 sensitive cells for each model in the last lines.
Parameters_EAICM-c_NON_resist_fit_Pr_only.mat	
Parameters_EAICM-af_NON_resist_fit_Pr_only.mat	
Parameters_EAICM-a_NON_resist_fit_Pr_only.mat	

Parameters_EAICM-cf_resist_fit_Pr_only.mat	} 12×300 table that gives the 8 reactions rates (10 for models without feedback loop) in the first lines and the 3 initial conditions obtained from the fit only on reaction rates for the 114 resistant cells for each model in the last lines.
Parameters_EAICM-c_resist_fit_Pr_only.mat	
Parameters_EAICM-af_resist_fit_Pr_only.mat	
Parameters_EAICM-a_resist_fit_Pr_only.mat	

Parameters_EAICM-cf_NON_resist_fit_Pi_only.mat	} 12×300 table that gives the 8 reactions rates (10 for models without feedback loop) in the first lines and the 3 initial conditions obtained from the fit only on initial conditions for the 300 sensitive cells for each model in the last lines.
Parameters_EAICM-c_NON_resist_fit_Pi_only.mat	
Parameters_EAICM-af_NON_resist_fit_Pi_only.mat	
Parameters_EAICM-a_NON_resist_fit_Pi_only.mat	

Parameters_EAICM-cf_resist_fit_Pi_only.mat	} 12×300 table that gives the 8 reactions rates (10 for models without feedback loop) in the first lines and the 3 initial conditions obtained from the fit only on initial conditions for the 114 resistant cells for each model in the last lines.
Parameters_EAICM-c_resist_fit_Pi_only.mat	
Parameters_EAICM-af_resist_fit_Pi_only.mat	
Parameters_EAICM-a_resist_fit_Pi_only.mat	

Parameters_EAICM-cf_NON_resist_fit_Pi_Pr.mat	} 12×300 table that gives the 8 reactions rates (10 for models without feedback loop) in the first lines and the 3 initial conditions obtained from the fit on both reaction rates and initial conditions for the 300 sensitive cells for each model in the last lines.
Parameters_EAICM-c_NON_resist_fit_Pi_Pr.mat	
Parameters_EAICM-af_NON_resist_fit_Pi_Pr.mat	
Parameters_EAICM-a_NON_resist_fit_Pi_Pr.mat	

Parameters_EAICM-cf_resist_fit_Pi_Pr.mat	} 12×300 table that gives the 8 reactions rates (10 for models without feedback loop) in the first lines and the 3 initial conditions obtained from the fit on both reaction rates and initial conditions for the 114 resistant cells for each model in the last lines.
Parameters_EAICM-c_resist_fit_Pi_Pr.mat	
Parameters_EAICM-af_resist_fit_Pi_Pr.mat	
Parameters_EAICM-a_resist_fit_Pi_Pr.mat	

With the same classification, the files that begin by "Reference.value" followed by the model's name, the cell fate ("resist" or "NON_resist") and the type of fit ("Pr_only", "Pi_only", "Pi_Pr"), contained 3 lines that gives the value of the slope, the C8 final value and the delay with T_{100000} in this order with as many columns as cells.